Proceedings of the ASME 2018 37th International Conference on Ocean, Offshore and Arctic Engineering
OMAE2018
June 17-22, 2018, Madrid, Spain

OMAE2018-77859

CONTROLLER ANALYSIS IN REAL-TIME HYBRID MODEL TESTING OF AN OFFSHORE FLOATING SYSTEM

Stefan A. Vilsen
Centre for Autonomous Marine Operations- and Systems (NTNU AMOS)
Department of Marine Technology
NO-7491 Trondheim, Norway
SINTEF Ocean
P.O. Box 4762 Torgard, NO-7465 Trondheim, Norway
Email: stefan.vilsen@sintef.no

Thomas Sauder
Centre for Autonomous Marine Operations- and Systems (NTNU AMOS)
Department of Marine Technology
NO-7491 Trondheim, Norway
SINTEF Ocean
P.O. Box 4762 Torgard, NO-7465 Trondheim, Norway
Email: thomas.sauder@ntnu.no

Martin Føre
Centre for Autonomous Marine Operations- and Systems (NTNU AMOS)
Department of Engineering Cybernetics
NO-7491 Trondheim, Norway
SINTEF Ocean
P.O. Box 4762 Torgard, NO-7465 Trondheim, Norway
Email: martin.fore@sintef.no

Asgeir J. Sørensen
Centre for Autonomous Marine Operations- and Systems (NTNU AMOS)
Department of Marine Technology
NO-7491 Trondheim Norway
Email: asgeir.sorensen@ntnu.no

ABSTRACT

This paper presents an experimental study using Real-Time Hybrid Model (ReaTHM) testing of a moored floating cylindrical buoy, conducted in a wave basin. ReaTHM testing is a method for studying the dynamics of marine structures by partitioning the system into numerical and physical substructures that are then coupled in real-time using a control system. In this study, the floating cylinder buoy is modelled physically, and the mooring system modelled numerically. In this paper, the effect of selected controller parameters on the performance of the control system is studied, for both wave frequency and low-frequency ranges. The architecture/design of the control system is presented in the first part of the paper, while results from experimental tests with wave excitation on the physical substructure are presented in the second part of the paper.

1 Introduction

The design processes for marine structures often requires model-scale testing to study complex hydrodynamic phenomena which are difficult to represent analytically or numerically (e.g. nonlinear wave loads, slamming or viscous effects). However, limitations arise when considering systems/structures in very deep water or with large geometric extent, such that scaling with conventional scaling methods becomes infeasible due to the high scaling ratio required [1].

Hybrid model testing methods have been suggested as a potential solution to mitigate such challenges, where the system under consideration is separated into physical and numerical substructures that are interconnected through a control system [2]. The method is inspired by similar methods developed and used in the civil engineering community [3] and automo-

tive/aerospace community [4]. The denomination Real-Time Hybrid Model testing (ReaTHM® testing[1]) is used by the authors when applying this method to problems within marine engineering. ReaTHM testing has primarily been used to apply numerically simulated wind forces to model scale testing of an offshore floating wind turbine [5, 6, 7]. Recent studies have aspired to develop such methods for applications with truncated mooring lines, both in numerical studies [8, 9] and in experimental applications [10, 11]. The long-term aim of these studies is to emulate systems that are of too large geometric extent to be implemented as a pure physical test setup in a test basin (e.g. Oil & Gas or fish production systems moored in deep water).

The present study represents the next step in this body of research and featured the laboratory setup developed and presented in previous studies [10]. Experiments were performed in the Marine Cybernetics Laboratory (MC Lab) at the Norwegian University of Science and Technology (NTNU), where the physical substructure was subjected to wave excitations.

A formal method for the design procedure of a ReaTHM test is submitted for publication in [12]. For the present setup, the initial design procedures for system identification and planning, model scaling and substructuring, and control system synthesis and design have been reported in [10]. The main scientific contribution of this study is the evaluation of how different controller components affect the performance of the actuation system when the physical substructure is exposed to large external disturbances from both Wave-Frequency (WF) and Low-Frequency (LF) motions.

The paper is organized as follows: the ReaTHM testing setup used in the experimental study is presented in Section 2, the results are presented and discussed in Section 3 while the conclusions are given in Section 4.

2 The ReaTHM test setup

The physical substructure was placed in the basin and attached with three actuation lines with 120 degree spacing, as illustrated in Figure 2.

2.1 Emulated system

The system under consideration (Emulated system), was an axisymmetric floating cylinder buoy, moored with a mooring system consisting of 12 mooring lines [10]. The substructuring was performed at the fairled point, such that the floating structure was modelled physically, while the mooring system was modelled numerically. The physical substructure was then scaled using Froude scaling and a scaling ratio $\lambda = 144$. Full scale and model scale parameters of the physical substructure are presented in Table 1. For simplicity, the mooring system was in this study

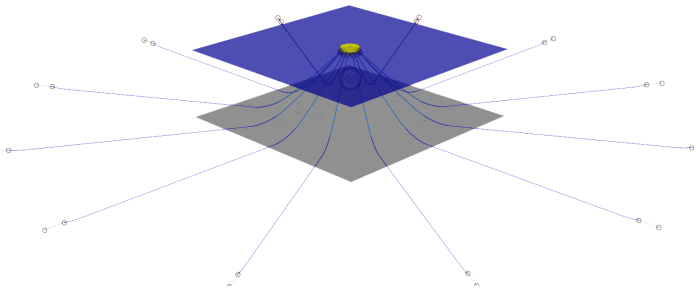

FIGURE 1: Emulated system under study.

TABLE 1: Main parameters of the physical system.

Cylinder Buoy	Full scale	Model scale
Radius [m]	43.2	0.30
Draft [m]	14.4	0.10
Volume [m^3]	$7.44 \cdot 10^4$	$2.49 \cdot 10^{-2}$
Mass [kg]	$8.62 \cdot 10^7$	28.2
Centre of gravity [m]	14.8	0.103
(height above keel)		
Metacentric height-Roll [m]	15.4	0.107
Metacentric height-Pitch [m]	15.3	0.106

reduced to a horizontal linear isotropic stiffness model, represented by $\tau = K \cdot \Delta$, where τ is the restoring force, K is the total horizontal mooring stiffness coefficient, and Δ is the excursion from the equilibrium point. It was then desired for the control system to apply the corresponding restoring force to the physical substructure when it was displaced from its equilibrium position.

2.2 Control system

The control system includes all system components necessary to connect the physical and numerical substructures, and had an overall structure as presented in Figure 3. The physical model was equipped with an optical position measurement system that measured the 6 Degrees Of Freedom (DOF) position and attitude by tracking three reflective markers attached to the buoy. A gyro for measuring rotation rates around the primary axis and an accelerometer that measured the 3DOF linear accelerations was mounted on the deck of the buoy.

The actuation system consisted of three DC motors placed around the basin with a 120 degree spacing. Each motor applied tension to the actuation line through a clock spring attached to a pulley wheel (Figure 2). The applied tension was measured by

[1]ReaTHM® testing is a registered trademark of SINTEF Ocean.

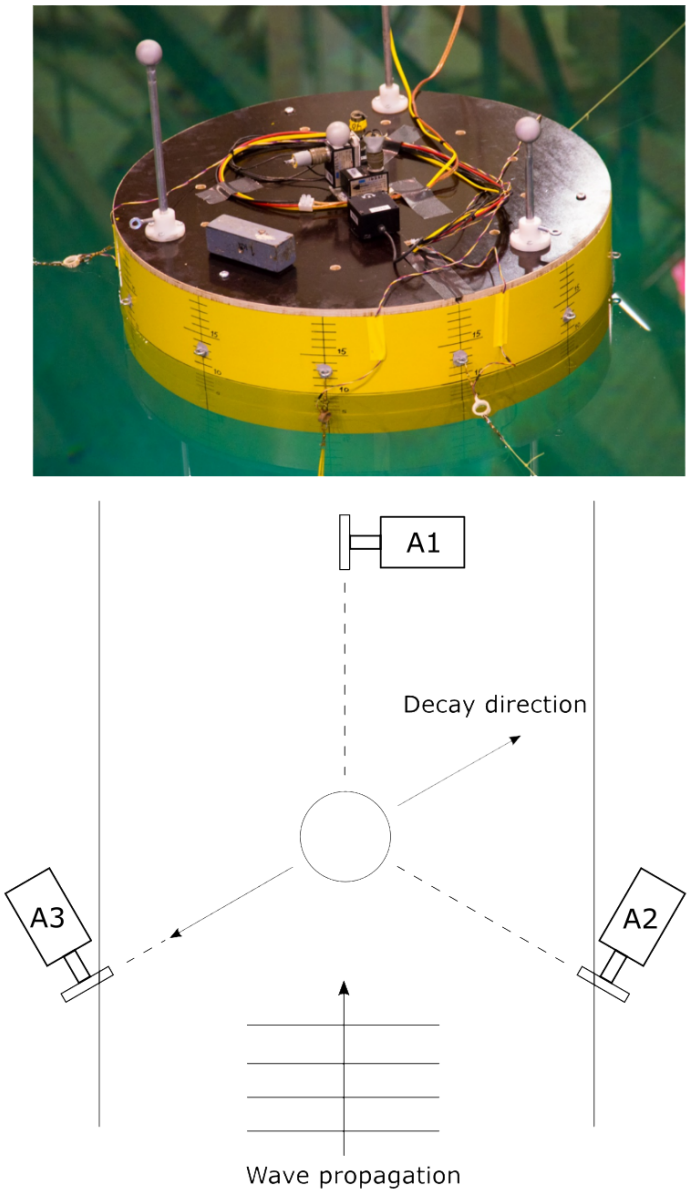

FIGURE 2: The physical substructure used in the tests (top). Layout of the experimental setup with actuator placement (bottom).

load cells on the physical model

A nonlinear passive observer for Inertial Measurement Unit (IMU) and Global Navigation Satellite System (GNSS) integration [13] was used to estimate the velocity based on the measured position and acceleration. The observer used the measured attitude (Euler angles) to rotate the body-fixed acceleration measurements into the local North-East-Down (NED) frame, and subtracting one g from the down axis to compensate for the gravity component of the acceleration.

The control strategy chosen for the system was to use the desired applied tension as control output and the motor position (i.e. the motor commands to actuators were given as angular positions of the motor shaft) as the control input. This meant that the first step of actuation was to convert the restoring force (τ_{ref}) output from the numerical model into desired line tensions (T_{ref}) for the three actuation lines using an allocation procedure [10]. The second step was then to compute the required motor command (θ_{cmd}), to apply the desired line tensions. This was done using a reference feed forward (rff) controller, that used a quasistatic model of the clock spring, actuation wheel and actuation line to estimate the motor command required to apply the tension output from the numerical model (θ_{rff}).

On the other hand, motions of the physical substructure, in turn, results in tension/relaxation of the actuation lines, exciting the clock springs attached to the actuators. The result is that a force which relates to the stiffness of the clock springs and the actuation lines, not to the stiffness of the numerical substructure, is applied to the physical substructure. To prevent such external disturbances from compromising the experimental outcomes, it is necessary to perform disturbance rejection [7]. This was ensured through a velocity feed forward (vff) controller, whose main control objective was to prevent that the motions on the physical substructure resulted in changes in the actuated load. From the estimated velocity of the physical substructure, the vff calculated the elongation velocities of the individual actuation lines. These were then integrated to find the motor command (θ_{vff}) required to compensate for the elongations and keep the applied tensions at the intended setpoint.

Finally, an integral feedback (ifb) controller was used to mitigate any drift, bias or errors not treated by the feed forward controllers. The ifb operated by integrating the error between the commanded and measured line tensions (θ_i). This control term was then added to the outputs from the rff and vff controllers, yielding the total motor command that was finally conveyed to the actuator (θ_{cmd}) according to

$$\theta_{cmd} = \theta_{rff} + \theta_{vff} + \theta_i \tag{1}$$

where

$$\theta_{rff} = (T_{ref} - T_0)\frac{-r}{k} \tag{2}$$

$$\theta_{vff} = r\int_0^t \dot{\delta}(t')dt' \tag{3}$$

$$\theta_i = K_i \int_0^t (T_{meas}(t') - T_{ref}(t'))dt' \tag{4}$$

T_{ref} is the desired reference tension output from the numerical model and allocation, T_0 is the pretension in the actuation lines, r

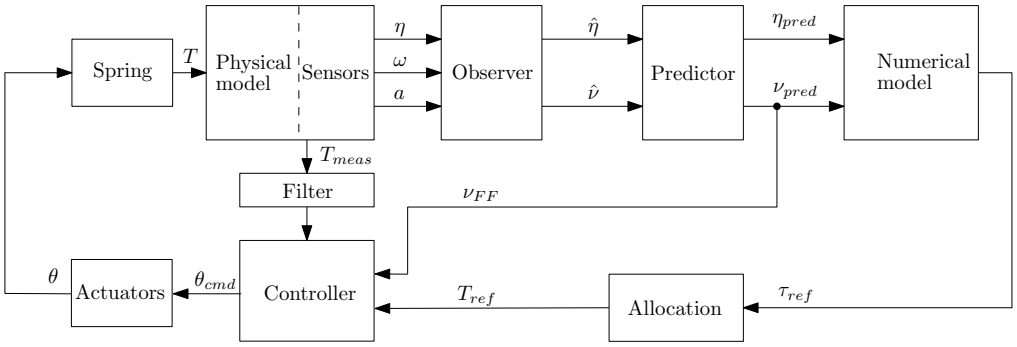

FIGURE 3: Control system structure for the hybrid test setup.

is the radius of the actuation wheel, k is the stiffness of the clock spring, $\dot{\delta}$ is the elongation velocity of the actuation line, K_i is the integral controller gain and T_{meas} is the measured line tension. Such a controller was used for each of the three actuators.

2.3 Performed tests

The initial controller and observer parameters previously tuned to give satisfactory results for decay testing in still water. The tests performed in this study used the base case parameters obtained from still water, but in all test cases the system was subjected to external disturbance from waves with wave height (H_s) of 0.01m and period (T) of 1 s (Table 2). This system was first subjected to a decay test where the buoy was manually moved 1.5 cylinder radius from the equilibrium and released (see table 2 for setup parameters). During this trial, the individual contributions from the different controllers to the final motor command, the commanded tension, and the measured actual tension were recorded. A series of experiments exploring the properties and limitations of the control system were then performed, in addition to the reference case setup. These tests included a variation of the integrator gain and pretension of the actuator lines, deactivation of the different components in the actuator control loop, and inducing artificial delays in observers and the numerical substructure. Pretension (T_0) was applied to the actuation lines to prevent the lines from going slack in case little or negative tension was commanded during testing. The required level of pretension is therefore normally determined by the expected variation in loading. A parameter study was performed here to evaluate the effect of varying the pretension level.

The time series of the error in the applied mooring load ($\tau_{meas}(t)$) from the desired mooring load ($\tau_{ref}(t)$), were evaluated by the standard deviation (σ) of the mooring load error (ε).

$$\varepsilon = \tau_{meas}(t) - \tau_{ref}(t) \tag{5}$$

To study the low frequency (typically caused by external disturbances such as wave excitations) and high frequency (typically due to control system) components of the errors separately, the total error was low pass and high pass filtered respectively, using a cutoff frequency of 5 Hz. Decay tests were performed in all cases except in a case when the actuators were deactivated, as decay tests were not possible without actuator action. Actuation was then deactivated by locking the motors at fixed positions, and the stiffness of the system was then solely determined by the stiffnesses of the clock springs in the actuators.

TABLE 2: Base case parameters.

H_s [cm]	T [s]	K_i [-]	T_0 [N]	K [N/m]
1.0	1.0	2.2	10	13.26

3 Results and Discussion

The applied tensions measured during the decay tests matched those commanded for the actuators. Results are presented for actuator three (Figure 4). This was also the case with the motor command signal (Figure 4), implying that the controllers were able to suppress the effects of external disturbances. It is apparent that the major component in the signal was disturbance rejection (the vff controller). The required motor command to apply the mooring load (rff controller) was relatively small, as the stiffness of the actuation system was much higher than the stiffness of the simulated mooring system. However, we can observe an error in the vff command, as the disturbance rejection is phase shifted compared to the motions of the physical substructure. Further, an overestimation of the velocity is seen to cause an overshoot in the vff signal. Both errors are seen to be corrected by the ifb controller, along with compensation for drift. The overshoot in vff signal causes an undershoot in the applied force, which is not fully compensated for by the ifb controller.

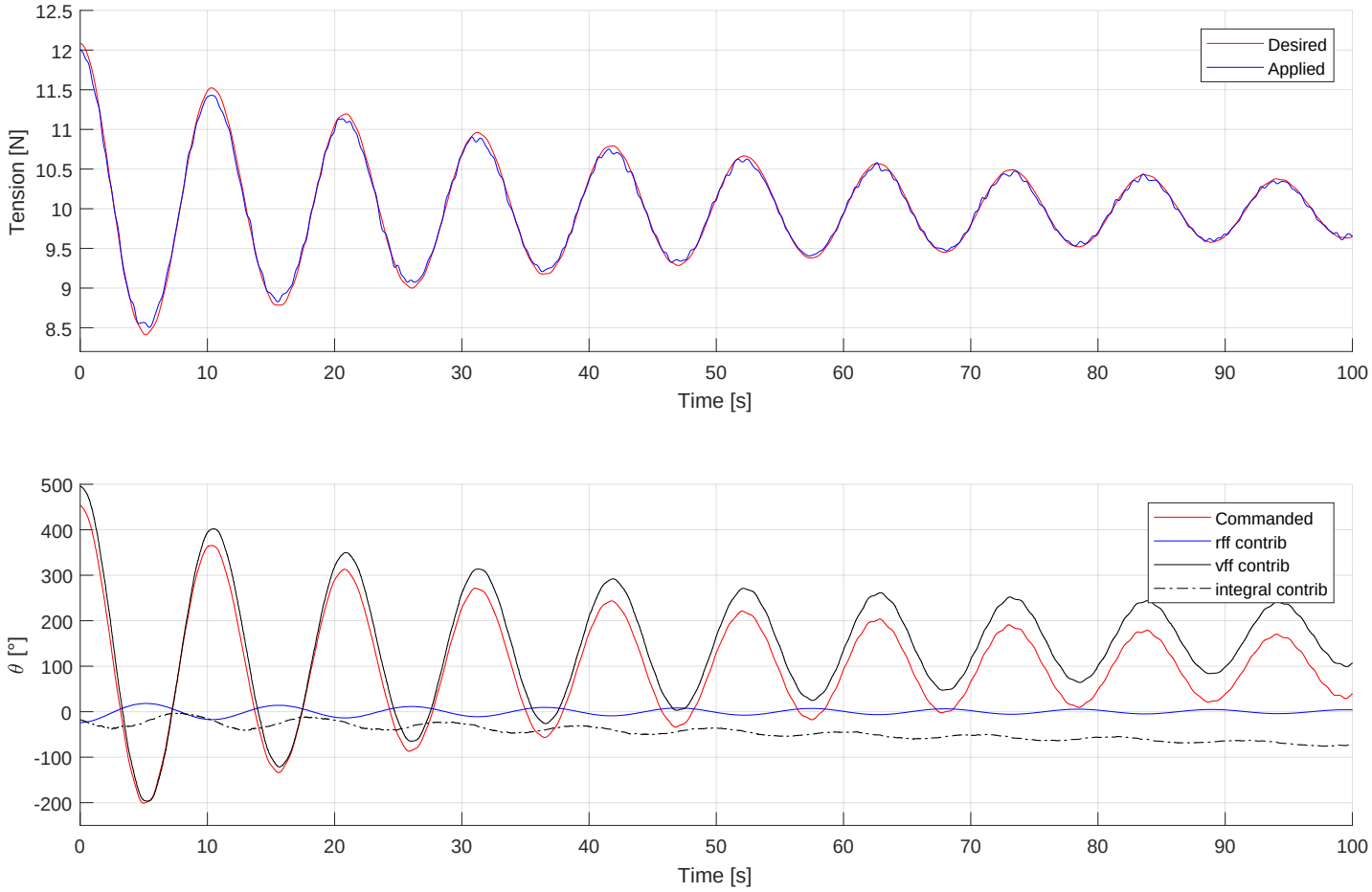

FIGURE 4: Desired and applied line tension for motor 3, during decay test with wave excitation (low-pass filtered with cutoff at 2 Hz) (top). individual controller commands for motor 3 (bottom).

LF components of the load error decreased with increased integrator gains, indicating that a high Ki gain is effective at suppressing the effects caused by external factors and slow varying modelling errors in the feed forward controllers (Figure 5a). This makes sense, as integral controllers are generally effective in removing bias and drift caused by slow varying loads. Conversely, the high-frequency noise component increased with increased Ki gain, possibly because the increased controller activity induced vibrations in the clock springs in the actuator system. Another explanation for this effect could be that faster integration action in combination with time delays in the actuation system may cause amplification of the high-frequency errors. Alternatively, the error may also have been increased by the velocity observer overestimating the changes in position, resulting in that the vff controller and the integral controller counteract each other, thereby limiting the efficiency of the integral controller.

The results from variation of the pretension (T_0) show that the total load error increases as the pretension is increased (Figure 5). This might be because higher pretension changes the Eigenvalues of the system and hence its response, or because a higher amplitude will amplify deviations.

Deactivation of the actuation led to very high load errors, but with a small high-frequency component compared with the base case (Figure 6). This implies that the control system action caused the high-frequency components in the tension error. The WF error constitutes the load error that needs to be compensated for by the disturbance rejection. Deactivating the vff controller was also expected to lead to higher LF error levels than in the base case, as most of the disturbance rejection abilities of the controller. While the LF error for this case was lower than in the case with no actuators, it was markedly higher than in the

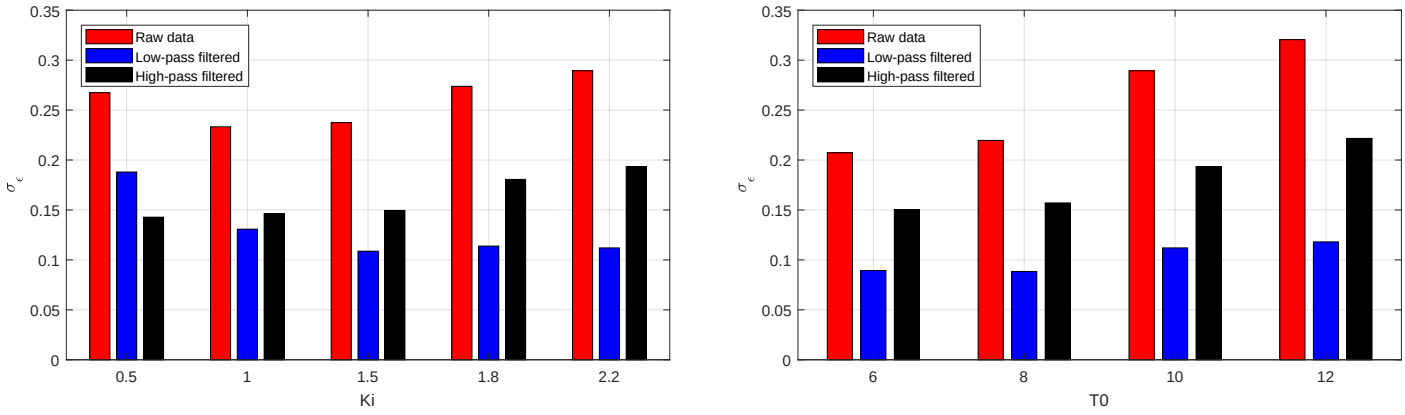

(a) (b)

FIGURE 5: Standard deviation of the error on the applied load as a function of integral controller gain (a) and pretension (b).

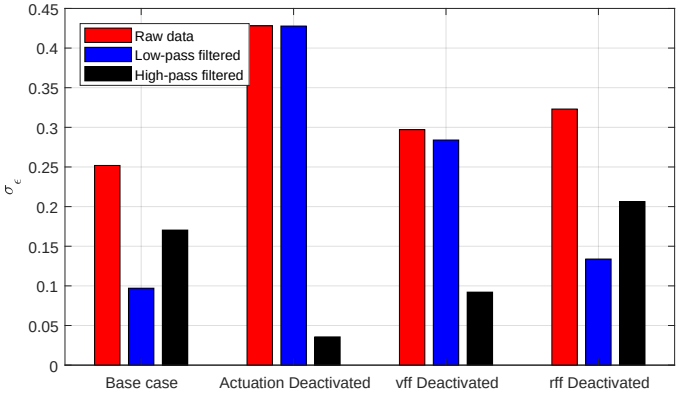

FIGURE 6: Evaluation of the effect of deactivating individual controller components.

base case (Figure 6). The effect of deactivating the rff controller differed from the other cases in that both high and LF error components were higher than in the base case. This was not unexpected as the rff controller was largely responsible for handling the conversion between desired loads and motor control signals. Deactivation would hence move more workload to the ifb controller and slow down the control reaction.

Introducing artificial delays on the inputs to the observer and numerical substructure generally led to increased error values (Figure 7). Time delays on input for the observer (Figure 7a) led to higher load errors than for time delay input on the numerical model (7b). This indicates that the present system is more sensitive to time delays on the observer inputs than on the numerical substructure input. A possible reason for this is that time delays on the observer input will affect the vff controller in addition to the numerical input. However, time delays on the numerical model input in general lead to challenges with e.g. negative damping [14].

4 Conclusions

This paper presented an application of Real-Time Hybrid Model testing to study of a moored floating structure. The effects of different controller components were evaluated through a parameter study with wave excitations. The vff controller used for disturbance rejection purposes was the dominating controller term. However, errors in the velocity estimation caused loss of performance of the vff term, and enforced the integral controller to correct the contribution from the vff. This is not ideal, both as high-frequency vibrations are induced by high integral gains, and undershoot/load errors was observed as a consequence. The system under study was scaled by a very high scaling ratio, and as such was very sensitive to errors. It is expected that some of the observed effects will be of less significance when applied to less sensitive test cases.

Acknowledgements

This work was supported by the Research Council of Norway through the Centres of Excellence funding scheme, Project number 223254 - AMOS, and through the project 254845/O80 "Real-Time Hybrid Model Testing for Extreme Marine Environments".

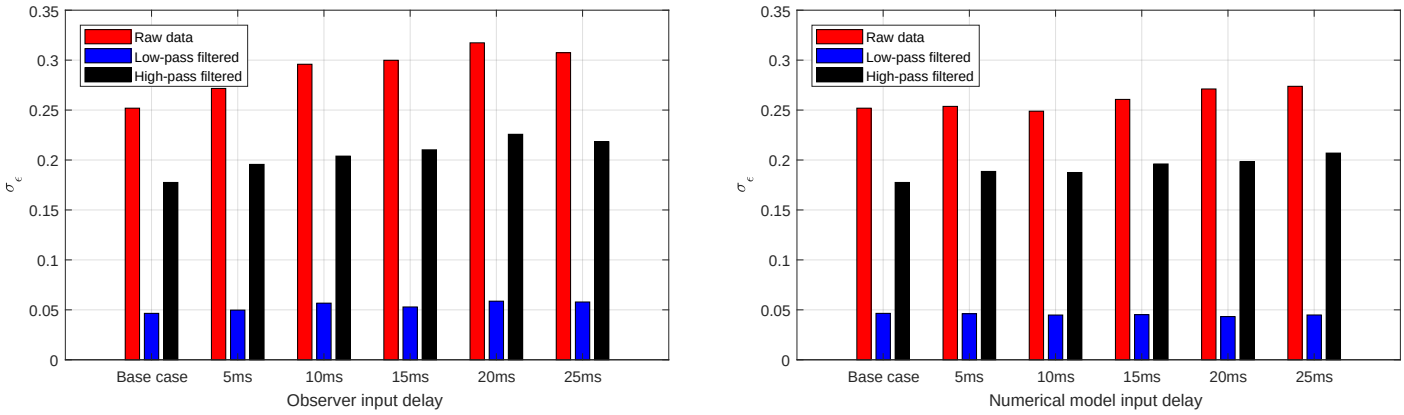

FIGURE 7: Evaluation of effect of delay on observer input (a) and numerical model input (B), low- and high-pass filtered at 0.5 Hz.

REFERENCES

[1] Stansberg, C. T., Ormberg, H., and Oritsland, O., 2002. "Challenges in deep water experiments: Hybrid approach.". *Journal of Offshore Mechanics and Arctic Engineering,* ***124***, pp. pp. 90–96.

[2] , 1998. Final report and recommendations to the 22nd ittc. Tech. rep., The ITTC Specialist Committiee on Deep Water Mooring.

[3] McCrum, D., and Williams, M., 2016. "An overview of seismic hybrid testing of engineering structures". *Engineering Structures,* ***118***, pp. pp. 240 – 261.

[4] Plummer, A. R., 2006. "Model-in-the-loop testing". *Proceedings of the Institution of Mechanical Engineers, Part I: Journal of Systems and Control Engineering,* ***220***(3), pp. pp. 183–199.

[5] Sauder, T., Chabaud, V., Thys, M., Bachynski, E., and Sæther, L., 2016. "Real-time hybrid model testing of a braceless semi-submersible wind turbine. part 1: The hybrid approach". *Proceedings of the ASME 2016 35th International Conference on Ocean, Offshore and Arctic Engineering*.

[6] Bachynski, E., Thys, M., Sauder, T., Chabaud, V., and Sætherr, L., 2016. "Real-time hybrid model testing of a braceless semi-submersible wind turbine. part 2: Experimental results". *Proceedings of the ASME 2016 35th International Conference on Ocean, Offshore and Arctic Engineering*.

[7] Chabaud, V., 2016. *Real-time hybrid model testing of floating wind turbines*. PhD thesis, Norwegian University of Science and Technology.

[8] Cao, Y., and Tahchiev, G., 2013. "A study on an active hybrid decomposed mooring system for model testing in ocean basin for offshore platforms". *Proceedings of the ASME 2013 32nd International Conference on Ocean, Offshore and Arctic Engineering*.

[9] Sauder, T., Sørensen, A. J., and Larsen, K., 2017. "Real-time hybrid model testing of a top tensioned riser: A numerical case study on interface time-delays and truncation ratio". *Proceedings of the ASME 2017 36th International Conference on Ocean, Offshore and Arctic Engineering*.

[10] Vilsen, S. A., Sauder, T., and Sørensen, A. J., 2017. *Real-time hybrid model testing of moored floating structures using nonlinear finite element simulations, "Dynamics of Coupled Structures, Volume 4"*. No. ISBN 978-3-319-54930-9. The Society of Experimental Mechanics, ch. 8, pp. 79–92.

[11] Vilsen, S. A., Føre, M., and Sørensen, A. J., 2017. "Numerical models in real-time hybrid model testing of slender marine systems". In Proceedings of the OCEANS'17 IEEE/MTS Conference, IEEE/MTS.

[12] Vilsen, S., Sauder, T., Sørensen, A. J., and Føre, M. "Method for real-time hybrid model testing of ocean structures: Case study on horizontal mooring systems". *Submitted for Publication, January 2018*.

[13] Fossen, T. I., 2011. *Handbook of Marine Craft Hydrodynamics and Motion Control*. No. 9781119991496. John Wiley & Sons, Ltd.

[14] Ueland, E. S., and Skjetne, R., 2017. "Effect of time delays and sampling in force actuated real-time hybrid testing; a case study". In Proceedings of the OCEANS'17 IEEE/MTS Conference, IEEE/MTS.